RSC Advances

PAPER

View Article Online
View Journal | View Issue

Cite this: *RSC Adv.*, 2015, **5**, 59070

Antibacterial properties of Ag–TiO_2 composite sol–gel coatings

E. Albert,[a] P. A. Albouy,[b] A. Ayral,[c] P. Basa,[d] G. Csík,[e] N. Nagy,[f] S. Roualdès,[c] V. Rouessac,[c] G. Sáfrán,[f] Á. Suhajda,[g] Z. Zolnai[f] and Z. Hórvölgyi*[a]

In this work the long-term antibacterial activity of silver doped titania coatings is studied systematically as a function of the titania layer structure (with and without molecular template) and the amount and physical properties of the silver dopant. Silver was incorporated in two different ways into the titania sol–gel films, either by co-deposition, *i.e.*, adding the silver ions directly to the precursor sol of the layer or by post-synthetic impregnation of the mesoporous titania coating. The structure and morphology of the layers were investigated using transmission and scanning electron microscopy, whereas the silver content was determined by Rutherford backscattering spectrometry. Antibacterial properties against *Escherichia coli* bacteria were studied by colony forming unit assay and agar diffusion method. It was found that directly after preparation, all composite coatings show antibacterial activity both in the dark and under visible light illumination. The antibacterial activity of the co-deposited samples vanished after the first use despite their high and constant remaining silver content (2.597 at%). This type of coating was not effective in agar diffusion tests at all. The antibacterial activity of the impregnated coatings with lower silver contents (0.596 at% and 1.961 at%), however, showed long-lasting antibacterial effect both in the colony forming unit assay and in agar diffusion tests as well. This can be attributed to the fact that the silver content is distributed over the mesoporous network of the titania coating and is effective during the long-term tests.

Received 3rd April 2015
Accepted 1st July 2015

DOI: 10.1039/c5ra05990a

www.rsc.org/advances

Introduction

Titania is widely used as a photocatalyst due to its effectiveness, chemical stability, non-toxicity, and relatively low cost. Since the first report on the antibacterial properties of a TiO_2 photocatalyst in 1985 (ref. 1) many studies have been presented on its antibacterial behaviour under different circumstances.[2–9] Due to its wide band gap (above 3.0 eV for rutile and 3.2 eV for anatase) TiO_2 can be applied only under UV irradiation. Solar light consists of about 5% UV and 45% visible light, therefore, the extension of the photocatalytic activity of TiO_2 to the range of visible light is desired.[2–4,10] A remarkable limiting factor of its capacity is the fast electron–hole recombination.[2,5,11–13] The visible light excitation of TiO_2 can be improved by applying dopants through changing its band structure.[2,4,9,14,15] Moreover, it was found that metal additives (*e.g.* Pt, Sn, Au, Ag) may enhance charge separation as well as by forming a Schottky barrier at the metal–photocatalyst interface.[2,6,12,16–19]

Silver is one of the most popular dopants thanks to its prominent antibacterial properties.[4,5,7,12,20–23] The mechanism of its antibacterial effect is generally proposed to the interactions between the silver compounds and the negatively charged bacteria cell wall membrane and DNA structure of bacteria.[2,5,24–29] As long as silver cations are known for a long time to be extremely toxic to bacteria cells,[26,30] silver nanoparticles have received great attention in the last decades.[26] Smaller size of silver nanoparticles results in higher specific surface area,[26,31] that allows higher silver ion release and easier interaction with other particles,[26,32] thus higher antimicrobial property. Silver is a well-known antibacterial material even in the absence of light, consequently, silver dopants broaden the bactericidal activity of photocatalyst composite materials, since their activity is usually limited to irradiation.[2,18] Furthermore, silver–titania composites can also act against silver-resistant microorganisms due to their photooxidative mechanism.[2,33]

Intensity of porous sol–gel coatings' investigations have recently increased in the field of protective thin films.[7,34–36] The

[a]*Budapest University of Technology and Economics, Department of Physical Chemistry and Materials Science, H-1521 Budapest, Hungary. E-mail: zhorvolgyi@mail.bme.hu; Fax: +36 1 463 3767; Tel: +36 1 463 2911*

[b]*Université Paris-Sud, Laboratoire de Physique des Solides, UMR 8502, F-91405 Orsay, France*

[c]*Institut Européen des Membranes, UMR 5635, University of Montpellier, F-34095 Montpellier, France*

[d]*Semilab Semiconductor Physics Laboratory Co. Ltd., H-1117 Budapest, Hungary*

[e]*Semmelweis University, Department of Biophysics and Radiation Biology, H-1444 Budapest, Hungary*

[f]*Hungarian Academy of Sciences, Centre for Energy Research, Institute of Technical Physics and Materials Science, H-1525 Budapest, Hungary*

[g]*Budapest University of Technology and Economics, Department of Applied Biotechnology and Food Science, H-1521 Budapest, Hungary*

antibacterial application of immobilized TiO_2 photocatalyst with high surface area – like mesoporous TiO_2 thin coatings – is more desirable than powdered catalysts[4,7,8] because of the difficulty of post-separation of the latter after the photoreaction.[4,37,38] From the point of view of practical applications, silver-based materials induce silver release. Consequently, lengthened antibacterial activity is a significant characteristic besides the high antibacterial efficacy.[2,4,5,39] Besides the advantage of providing high surface area for the composite material, the pore structure of mesoporous TiO_2 coatings can serve as silver carrier as well.[7] From this brief overview it can be seen that the details and supposed mechanisms of photocatalytic activity are widely studied. The antibacterial effect of silver nanoparticles[5,22–26] and their combination with TiO_2 (ref. 2–8 and 12) were also investigated from numerous aspects. Despite the great deal of research done on silver doped antibacterial TiO_2 coatings, studies correlating material properties, amount and occurrence of the dopant with the short- and long-term antibacterial activity are rare.

In this study we investigate the connection between the applied silver-doping method, the resulting nature and amount of the silver dopant together with the structural properties of the composite coatings and the long-term antibacterial activity of TiO_2 thin films. For this purpose TiO_2 sol–gel coatings were prepared on glass substrates applying dip-coating technique. Silver was incorporated into the coatings in form of $AgNO_3$ by two different ways: by adding it to the components of the precursor sol or by impregnation of the ready-made mesoporous TiO_2 coatings with $AgNO_3$ solution – utilizing the particle size limiting character of the mesopores.

TiO_2 coatings were obtained by using titanium(IV) butoxide or titanium(IV) isopropoxide as precursor and cetyltrimethylammonium bromide as templating agent for porous coatings. Structural and surface properties were investigated by transmission electron microscopy, scanning electron microscopy, and ellipsometric porosimetry. The crystal structure of the TiO_2 coatings was determined by wide-angle X-ray scattering analysis and high resolution transmission electron microscopy. Silver content of the coatings was measured by Rutherford backscattering spectrometry. The antibacterial behaviour of the samples against *Escherichia coli* bacteria was studied by colony forming unit assay and agar diffusion method as well.

Experimental

Materials

Titanium(IV) butoxide (TBuOTi, for synthesis, ≥98%, Merck), titanium(IV) isopropoxide (TIsoPrOTi, 98+%, Acros Organics), ethanol (EtOH, a.r., >99.7%, Reanal), 2-propanol (2-PrOH, a.r., >99.7%, Reanal), nitric acid (HNO_3, special grade, 65%, Lach-Ner), acetic acid (AcAc, G. R., 99.8%, Lach-Ner), cetyltrimethylammonium bromide (CTAB, cationic surfactant, 99+%, Acros Organics), and distilled water (H_2O, 18.2 MΩ cm, purified with a Millipore Simplicity 185 filtration system) were used as starting materials for precursor sol synthesis. Silver nitrate ($AgNO_3$, G. R., 99.9%, Lach-Ner) was used for the preparation of silver containing coatings.

Microscope glass slides (76 × 26 × 1 mm, Thermo Scientific, Menzel-Gläser) and silicon (Si) wafers were applied as solid substrates of the coatings. Solid substrates were cleaned using 2-propanol (2-PrOH, a.r., >99.7%, Reanal) and distilled water (H_2O, 18.2 MΩ cm, purified with a Millipore Simplicity 185 filtration system).

The antibacterial activity of the prepared samples was studied by using *Escherichia coli* B. ATCC 11303 bacteria strain, brain heart infusion broth (DifcoR), nutrient broth for microbiology (Sigma-Aldrich), sodium-chloride (NaCl, a.r., Reanal). Phosphate buffer solution (pH = 7.4) was prepared using the following materials: magnesium sulfate ($MgSO_4$, Pharmacy of SOTE University), ammonium chloride (NH_4Cl, alt. Reanal), potassium dihydrogen phosphate (KH_2PO_4, a.r. Reanal), and disodium hydrogen phosphate (Na_2HPO_4, alt., Reanal).

Synthesis of precursor sols

Titania precursor sol (*precursor sol* (*1*)) was prepared *via* the acid catalyzed controlled hydrolysis of titanium(IV) butoxide in ethanolic media. Nitric acid was used as catalyst during the synthesis of precursor sol. The molar ratios for TBuOTi : EtOH : HNO_3 : H_2O were 1 : 27.95 : 0.49 : 0.82.

In order to obtain mesoporous titania coatings, surfactant containing precursor sol (*precursor sol* (*2*)) was prepared by adding CTAB into the mixture of *precursor sol* (*1*). The molar ratios for TBuOTi : EtOH : HNO_3 : H_2O : CTAB were 1 : 27.95 : 0.49 : 0.82 : 0.125.

The obtained mixtures (both *precursor sol* (*1*) and *precursor sol* (*2*)) were stirred for 2 hours at 60 °C.[40]

Silver containing titania coatings were obtained by two different ways: by immersing the ready-made mesoporous titania coatings in an aqueous $AgNO_3$ solution or by adding $AgNO_3$ into the precursor sol (in the case of *precursor sol* (*3*)).

Precursor sol (*3*) was prepared by the acid catalyzed controlled hydrolysis of titanium(IV) isopropoxide in 2-propanol in the presence of AcAc as catalyst and $AgNO_3$ at room temperature similarly as presented by Tomás *et al.*[41] The molar ratios for TIsoPrOTi : 2-PrOH : AcAc : H_2O : $AgNO_3$ were 1 : 3.72 : 1.89 : 1.87 : 0.1.

Preparation of samples

Microscope glass slides and in certain cases silicon (100) wafers were used as solid substrates for layer deposition. Prior to film deposition solid substrates were erased with 2-propanol impregnated cotton, then rinsed with 2-propanol and distilled water. Both glass and silicon substrates were dried at room temperature before using.

Sol–gel coatings on solid substrates were prepared from the precursor sols by the dip-coating method. A dip coater (built in MTA MFA, Hungary) was used for layer deposition. Cleaned and dried substrates were immersed into the precursor sol and pulled out with a constant speed of 12 cm min^{-1} (*precursor sol* (*1*) and *precursor sol* (*2*)) or 2 cm min^{-1} (*precursor sol* (*3*)).

The deposited films were annealed in a drying oven (Nabertherm B170) at 450 °C for 30 minutes in case of samples (*TiO_2* and *$pTiO_2$*) prepared from *precursor sol* (*1*) and *precursor*

Table 1 Summary of sample preparation and notations (p = molecular-templated porous)

Sample notation	Precursor sol/CTAB	Silver additive	Way of silver incorporation
TiO_2	(1)/—	—	—
$pTiO_2$	(2)/CTAB	—	—
$pTiO_2$–0.03 M $AgNO_3$	(2)/CTAB	0.03 M $AgNO_3$	Impregnation into the pores
$pTiO_2$–1 M $AgNO_3$	(2)/CTAB	1 M $AgNO_3$	Impregnation into the pores
$pTiO_2$–2*1 M $AgNO_3$	(2)/CTAB	1 M $AgNO_3$ twice	Impregnation into the pores, twice
TiO_2–$AgNO_3$	(3)/—	$AgNO_3$	Addition to the precursor sol

sol (*2*), respectively. Coatings (*TiO_2–$AgNO_3$*) obtained from *precursor sol* (*3*) were heat treated in two steps: samples were treated at 60 °C for 30 minutes which was followed by annealing them at 450 °C for 30 minutes. The heating rate was 5 °C min^{-1} in all cases.

Silver containing mesoporous titania coatings (*$pTiO_2$–$AgNO_3$*) were obtained by the impregnation of $AgNO_3$ solution into the porous structure of the ready-made coatings using the dip coater. Aqueous $AgNO_3$ solutions were applied in two different concentrations: 0.03 M and 1.0 M. In order to avoid the formation of air inclusions in the pores, the mesoporous titania coatings were immersed into the $AgNO_3$ solution with a slow constant speed of 1 cm min^{-1}. The withdrawal speed was 12 cm min^{-1}. Then the surface of the samples was rinsed with distilled water and dried at room temperature. In order to reduce the Ag^+ ions to Ag^0 the same heat treatment was applied like in the case of *TiO_2–$AgNO_3$* type coatings. Silver containing mesoporous titania samples with higher silver concentration (*$pTiO_2$–2*1 M $AgNO_3$*) were prepared by two consecutive applications of the immersion of porous samples into the 1.0 M $AgNO_3$ solution. In the latter case heat treatment was applied after both immersions. Table 1 summarizes the main parameters of sample preparation and sample notations.

Investigation methods

Wide-angle X-ray scattering analysis. All types of the coatings were prepared on (100) Si substrates and doped with silver as described above. The two-dimensional wide-angle X-ray scattering (WAXS) patterns were collected on a MAR345 detector using Cu-Kα radiation (wavelength: 1.542 Å) of a rotating anode X-ray source (40 kV, 40 mA; multilayer graded monochromator). Exposure time is 1800 s and the 2θ-value is 30° at the image centre.

Characterization of coatings by ellipsometric porosimetry. Ellipsometric porosimetry (EP) measurements were carried out by a Semilab's PS-2000 apparatus. EP is a technique suitable for characterizing porous thin films for open porosity, surface area, pore size, and mechanical strength. EP is a coupled technique in which the vapour adsorption can be studied step-by-step through spectroscopic ellipsometry. During the measurement vapour of the adsorptive material condenses in the pore system which induces effective refractive index shift. Measuring the adsorption and the desorption isotherms the porosity of the sample can be determined, furthermore, the pore size distribution can be calculated based on the modified Kelvin equation in case of mesopores (pore size ranging from 2 nm to 50 nm). *TiO_2*, *$pTiO_2$*, and *TiO_2–$AgNO_3$* type coatings deposited onto Si substrates were characterized by this method using toluene as adsorptive material. Before the measurement the samples were heated up to 448 K for 20 minutes. The toluene adsorption isotherms were taken at 294 K. Furthermore, EP provides the possibility to determine the optical properties of the samples as a spectroscopic ellipsometer at zero relative pressure of the adsorptive material. The measurements were carried out at the angle of incidence of 60° in the wavelength range of 173.6–9714.5 nm. The thickness and the effective refractive index of the coatings were determined by applying the Tauc–Lorentz oscillator model successfully in the full wavelength range.

Characterization of coatings by field emission scanning electron microscopy. Coatings prepared onto silicon wafers were studied with field emission scanning electron microscopy (FESEM) as well. Top view and cross-sectional images were taken using a LEO 1540 XB scanning electron microscope applying 5.00 keV acceleration voltage. Cross-sectional images were also used for the determination of layer thicknesses.

Characterization of the coatings by transmission electron microscopy. Samples deposited on silicon substrates were prepared in cross-section for transmission electron microscopic (TEM) and high-resolution transmission electron microscopic (HRTEM) investigations by conventional mechanical and ion beam thinning techniques. The morphology and structure of the coatings was investigated by a 300 kV JEOL 3010 HRTEM with a point resolution of 0.17 nm. The microscope was equipped with a Tridiem GATAN Image Filter (GIF) that was used for energy filtered TEM imaging by selecting various regions of the electron energy loss (EELS) spectrum. The EELS spectrum arises due to the energy loss of the electrons of the illuminating beam that interact with the sample during transmission. Some of the electrons undergo inelastic scattering and lose energy. Inelastic interactions include phonon excitations, inter and intra band transitions, plasmon excitations, inner shell ionizations, *etc.* The energy loss can be measured and analysed in detail by EELS spectrometry. In addition to EELS spectrometry, image filtering can be applied to compose images by using electrons that have lost certain amount of energies. In the present work we applied the image filter (GIF) for taking "zero-loss" and "plasmon images". The contrast of zero-loss imaging is similar to that of conventional TEM imaging, while plasmon imaging

enables the discrimination of conductive and non-conductive (metal and insulator) parts of the sample.

Rutherford backscattering spectrometry. Rutherford backscattering spectrometry (RBS) measurements were carried out in order to determine the silver content of the coatings prepared on top of silicon wafers. RBS analysis was performed in a scattering chamber with a two-axis goniometer connected to a 5 MV Van de Graaff accelerator. The 1 MeV $^4He^+$ analyzing ion beam was collimated with two sets of four-sector slits to the dimensions of 0.5 × 0.5 mm^2, while the beam divergence was kept below 0.06°. The beam current was measured by a transmission Faraday cup. In the scattering chamber the vacuum was about 1×10^{-4} Pa. To reduce the hydrocarbon deposition, liquid N_2 cooled traps were used along the beam path and around the wall of the chamber. Backscattered He^+ ions were detected using an ORTEC surface barrier detector mounted in Cornell geometry at scattering angle of $\theta = 165°$. The energy resolution of the detection system was 16 keV. Spectra were recorded at sample tilt angles of 7° and 60°. In all experiments both axial and planar channeling of the He^+ projectiles in the single crystalline Si substrate was avoided. The measured RBS spectra were evaluated with the RBX[42] spectrum simulation code.

Study of the antibacterial activity. Antibacterial activity of the coatings (prepared onto glass substrate) against *Escherichia coli* bacteria (ATCC 11303) was studied by two different antibacterial tests: the colony forming unit (CFU) assay and the agar diffusion method. The CFU assay is a quantitative method, while the agar diffusion test is a semi-quantitative one. CFU assay shows the viability of bacterial cells after being incubated on the surfaces with sol–gel coatings. Here the bacterial cells can only be inactivated by a contact mechanism. However, bacterial inactivation due to both contact and diffusion mechanism can be evaluated using the agar diffusion method.

Escherichia coli cells were grown aerobically in a brain heart infusion broth containing 0.5% NaCl. The cultures were kept under aerobic conditions for 12 hours at 37 °C. 5 mL of the overnight culture were transferred into 45 mL fresh medium and grown to log phase. The typical cell concentration was 1×10^8 cells per cm^3.

In the case of CFU assay, *Escherichia coli* cells were incubated on the surface of the prepared samples in the dark or under white light irradiation. Irradiation was carried out using a 60 W lamp (General Electric, 400–1000 nm, 2.93 mW cm^{-2}) at 20 cm distance from the samples. Three parallel coatings were studied in each case and experiments were repeated three times for each type of sample. A cleaned bare glass substrate kept under the same conditions like the investigated samples was used as control sample during all antibacterial experiments. After one-hundred-fold dilution of log phase bacterial suspension with phosphate buffer solution, 200 μL of the suspension was spread onto the surface of the investigated and control samples. After 2 hours aliquots were taken from the treated and control cell suspensions. After serial dilution in phosphate buffer solution, cells were spread out onto agar plates made of brain heart infusion with 0.5% NaCl, added to 1.5% purified agar. Three parallel aliquots were taken for spreading from each diluted cell suspension. Thus, 9 parallel CFU values were obtained for each type of sample. The number of CFUs was determined after an incubation period of 24 hours at 37 °C. The survival fraction was calculated using $(N/N_0) \times 100$, where N_0 and N are the average number of CFUs obtained for the control glass substrate and for the investigated sample, respectively.

In the case of agar diffusion test *Escherichia coli* bacteria containing agar plates were obtained by mixing 1 mL of the tenfold diluted bacterial suspension with 10 mL nutrient agar at 45 °C. The investigated samples were placed onto the surface of the agar plates. The presence and the extent of the inhibition zone around the samples were studied after incubation for 24 hours at 37 °C.

The durability of the silver containing titania coatings was also studied. The repeated antibacterial application of the samples was studied by experimental modelling: 200 μL of the phosphate buffer solution (not containing bacteria cells) used during the CFU assay was spread and kept on the surface of the titania coatings for 2 hours and 20 hours. Similarly, in case of agar diffusion experiments the samples were immersed into *ca.* 9 mL buffer solution and kept in it for 2 hours and 20 hours. The buffer solution was changed to fresh on the surface or around the sample after every 2 hours. Finally, the samples were rinsed with distilled water and dried for 1 hour at 120 °C that was followed by the agar diffusion test and CFU assay carried out in dark as presented above. The aim of this investigation was to study the role of the released silver in the antibacterial behaviour of the samples and hereby the durability of these types of samples. Parallel of the antibacterial tests the silver content of the as prepared and of the soaked coatings was determined by RBS.

Results and discussion

Crystalline structure of TiO_2 by wide-angle X-ray scattering analysis

All types of titania coatings were prepared on (100) Si substrates and doped with silver as described above. The two-dimensional WAXS patterns and the corresponding radial scans are shown in Fig. 1 for TiO_2 and $pTiO_2$ type coatings. The marked peaks at the angle of $2\theta = 25.84°$, 48.34°, and 38.19° are associated to the following *d*-spacings: 3.45 Å, 1.88 Å, and 2.36 Å, respectively. They compare well to the values given for the three most intense diffraction lines in anatase: 3.51 Å, 1.891 Å, and 2.379 Å (see the Powder Diffraction File card 21-1272 or http://www.webmineral.com).

The anatase form was expected based on the temperature of the thermal annealing applied at sample preparation.[40] This fact is important also from the point of view of photocatalysis due to the highest activity of the anatase form.[43] Similar results were obtained for the other silver-doped coatings. The most intense diffraction line for silver particles is expected at $2\theta \approx 38°$ ((111) indices). TEM images evidence nanoparticles too large to evoke line broadening as an explanation of the absence on measurable signal around this angle. A better explanation is most probably too low a nanoparticle concentration combined with an intense background (essentially air scattering). The strong and slightly structured background originates from the (100) Si substrate (thermal scattering).

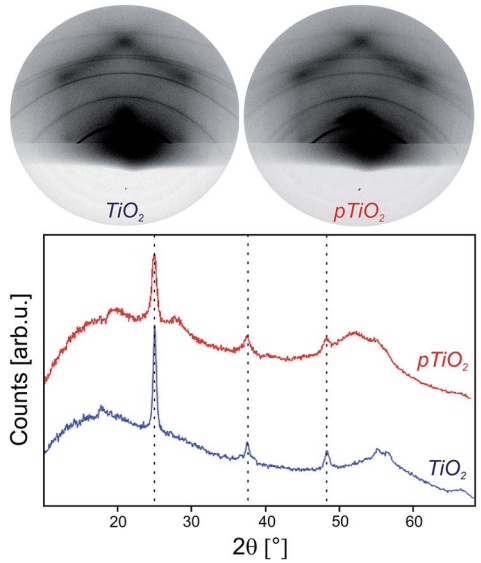

Fig. 1 WAXS 2D-patterns and corresponding diagrams of TiO_2 and $pTiO_2$ type coatings. The diagram is shifted along the counts axis for better visibility. The strong background originates from the (100) Si substrate.

Ellipsometric porosimetry measurements

TiO_2 and $pTiO_2$ coatings deposited onto silicon substrates were characterized by ellipsometric porosimetry measurements to investigate the amount and character of the available open pores. The adsorption and desorption isotherms presented in Fig. 2(a), (c) and (e) were taken at 294 K using toluene as adsorption material. The normalized pore radius distribution of the pore systems was determined by using the modified Kelvin equation and assuming cylindrical pores. They are presented in Fig. 2(b), (d) and (f).

All sorption isotherms are similar in shape to type IV in IUPAC classification terms[44] referring the mesoporous character of the coatings. The hysteresis loops are of type H2, according also to IUPAC classification. It corresponds to materials with interconnected pore system and non-uniform pore sizes. The TiO_2 type samples have larger hysteresis cycle (Fig. 2(a)) compared to the $pTiO_2$ (Fig. 2(c)). It refers that these samples contain mesopores interconnected by relatively narrow pore openings while the $pTiO_2$ type coatings have not so narrow windows. In case of TiO_2–$AgNO_3$ type samples (Fig. 2(e)) adsorption occurs also at higher relative pressure values (up to 0.65) compared to the previous two samples (0.45). It corresponds to the existence of pores with larger diameter which appear in the pore radius values in Table 2. The thickness and the effective refractive index of the coatings were also determined by applying the Tauc–Lorentz oscillator model at zero relative pressure of the adsorptive material. The optical properties are also collected in Table 2.

Scanning electron microscopy measurements

Fig. 3 shows the representative top-view and cross-sectional FESEM images of various types of titania coatings deposited onto Si substrates.

It can be seen that the coatings cover entirely the surface of the Si substrates in all cases, resulting in coatings with smooth surfaces. The TiO_2 type coating's thickness is 68 nm determined from the cross-sectional analysis (Fig. 3(a)). This value is in close agreement with that obtained by analysing the spectroscopic ellipsometric curves (Table 2) of the same types of coatings. Studying the images taken about the TiO_2 type coating (Fig. 3(a)) it can be seen that the structure of the coating is not entirely compact, one kind of porosity is observable that corroborates the porosity values obtained from the ellipsometric porosimetry measurements.

For $pTiO_2$ type sample (Fig. 3(b)) the thickness of the coating was determined to be 86 nm which is also in close agreement with the results of ellipsometric analysis (82 nm). Regarding the structure of the impregnated $pTiO_2$ type sample the porous structure of the coating is observable both in top-view and cross-sectional images, but the size of the pores is small to resolve and measure it by FESEM.

The silver content of the $pTiO_2$–1 *M* $AgNO_3$ cannot be unambiguously identified either in top-view or in the cross-sectional image, *i.e.*, no difference can be observed between the images taken of $pTiO_2$ and $pTiO_2$–1 *M* $AgNO_3$ type samples. It refers that there are not Ag particles on the surface or their size is smaller than the resolution limit (*ca.* 5 nm). Considering the cross-sectional image the mesopores probably provided their size-limiting function during the Ag accumulation.

Contrarily, the surface of TiO_2–$AgNO_3$ type samples (Fig. 3(c)) carries several variously shaped Ag-particles with various dimensions. Besides the few particles with small diameter less than 50 nm, the typical size of the most particles is about 100 nm, or more.

Transmission electron microscopy analysis

The TEM investigations revealed the morphology and structure of TiO_2, $pTiO_2$–1 *M* $AgNO_3$ and TiO_2–$AgNO_3$ type samples. Due to the applied preparation technique TiO_2 and $pTiO_2$–1 *M* $AgNO_3$ type samples were prepared for cross-sectional TEM analysis simultaneously.

The cross sectional images in Fig. 4(a) and (b) show that the thickness of TiO_2 and $pTiO_2$–1 *M* $AgNO_3$ type samples are 58 nm and 88 nm, respectively. Both layers are crystalline titania with numerous pores. The distribution and size of pores in these films seem to be uniform. It is supported by both the contrast features of the TEM zero loss image in Fig. 4(a) and the picture taken with the plasmon energy loss of 26 eV of the EELS spectrum Fig. 4(b). Here the dark contrast spots on the top and inside the $pTiO_2$–1 *M* $AgNO_3$ type sample represent metallic behaviour, *i.e.*, the presence of Ag grains, while in TiO_2 type sample the dark spots (Ag) are missing.

TiO_2–$AgNO_3$ type sample is represented by Fig. 4(c) and (d). This layer shows pore structure different from TiO_2 and $pTiO_2$–1 *M* $AgNO_3$ type samples, *i.e.*, the local distribution and size of pores is variable in TiO_2–$AgNO_3$ type sample. The regions filled with Ag appear also as percolated as shown by both the TEM zero loss image (Fig. 4(c)) and by the plasmon image (Fig. 4(d)). In this plasmon image the dark contrast features represent an

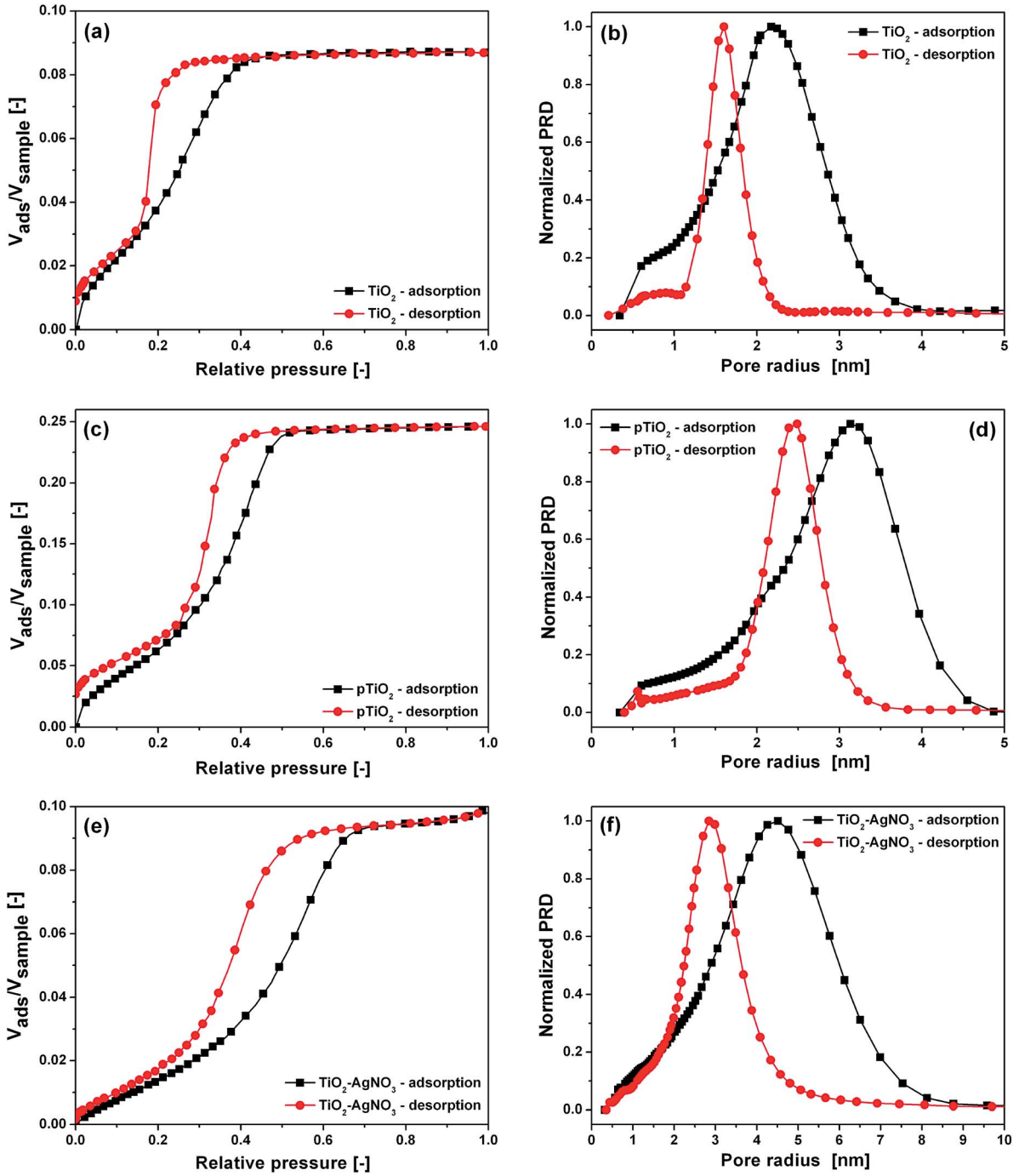

Fig. 2 Toluene adsorption–desorption isotherms at 294 K and normalized pore radius distribution of (a and b) TiO_2, (c and d) $pTiO_2$, and (e and f) TiO_2–$AgNO_3$ type titania coatings determined by ellipsometric porosimetry.

uneven distribution of Ag. The irregular pore structure and distribution of Ag is attributed to the preparation technique different from TiO_2 and $pTiO_2$–*1 M* $AgNO_3$ type samples.

HRTEM was applied on $pTiO_2$–*1 M* $AgNO_3$ and TiO_2–$AgNO_3$ type samples to reveal the actual phase of the titania films. Three possible polymorphs, rutile, anatase and brookite, of the titania were suggested as composing the layers. Fig. 4(e)–(h) show high resolution images and the representative Fast Fourier Transforms (FFT) of $pTiO_2$–*1 M* $AgNO_3$ and TiO_2–$AgNO_3$ type sample, respectively. According to the PCPDF database (a database of International Centre for Diffraction Data) the three polymorphs have numerous overlapping lattice spacings. The determined period of 0.352 nm may correspond to the 101 lattice planes of bct anatase (PCPDF 84-1285) or the 210 planes of brookite (PCPDF 76-1937). This lattice period was found in all areas of our samples. The analysis of HRTEM micrographs and their Fast Fourier Transforms (FFT) revealed that our films build up typically from anatase. In addition, the 111 lattice

Table 2 Layer thicknesses, effective refractive indices, porosity, and pore radius values of TiO_2, $pTiO_2$, and TiO_2–$AgNO_3$ type coatings determined by ellipsometric porosimetry

Sample	Thickness [nm]	Effective refractive index @ 632.8 nm	Porosity [%]	r_{ads} [nm]	r_{des} [nm]
TiO_2	64	2.215	8.7	2.2	1.6
$pTiO_2$	82	1.823	24.6	3.1	2.5
TiO_2–$AgNO_3$	96	2.235	9.8	4.5	2.8

period of fcc Ag (0.232 nm, PCPDF 84-1285) measured in the protruding Ag grains in Fig. 4(e) and (f) was used for a calibration of the measurement. The fringes with 2–5 nm period that appear in the HRTEM image in Fig. 4(f) are Moire patterns that arise due to the combination of lattice fringes of overlapping crystals.

Antibacterial activity of the samples

For studying the role of direct contact and diffusion mechanism in the antibacterial activity, investigations were carried out by the colony forming unit assay and agar diffusion method, respectively.

Results of the colony forming unit assay. Antibacterial behaviour of all types of samples was studied against *Escherichia coli* bacteria in the dark and under visible light irradiation (60 W lamp, 400–1000 nm, 2.93 mW cm^{-2}, 20 cm) by the CFU assay. The contact time of the bacterial suspension with the surface of the samples was 2 hours. A cleaned glass substrate that was treated identically like the coated samples was used as reference sample during all experiments. Fig. 5(a) and (b) show the representative results of the CFU assay antibacterial tests carried out in the dark and under visible light illumination, respectively.

Although the coatings without silver additive (TiO_2 and $pTiO_2$) show antibacterial effect both in the dark and upon irradiation, the effect increases significantly by the incorporation of silver into the coatings. For porous coatings impregnated with $AgNO_3$ the antibacterial behaviour correlates with the presumed silver content of the coatings but there is no significant difference in the activity of the samples impregnated ones ($pTiO_2$–*1 M* $AgNO_3$) and twice ($pTiO_2$–*2*1 M* $AgNO_3$).

Comparing the antibacterial effect of the coating prepared by adding $AgNO_3$ into the precursor sol (TiO_2–$AgNO_3$) with the impregnated ones, it can be seen that despite the expectedly higher silver content, TiO_2–$AgNO_3$ samples do not show increased antibacterial activity either in the dark or upon irradiation. The explanation can be found in the difference of the nature of Ag nanoparticles revealed by FESEM, HRTEM, and EELS analysis. In case of impregnated samples the Ag-content is located in the pore structure with small dimensions. The diameter of few larger particles grew on the surface is less than 15 nm, while the surface of TiO_2–$AgNO_3$ type sample carries several crystalline particles with various diameters. Besides the few particles with small diameter less than 50 nm, the typical dimension of the most particles is about 100 nm, or more. It seems that a significant part of the Ag-content is represented by these large particles, however, the Ag-islands in the coating material have smaller dimensions. Several study showed that the antimicrobial activity of smaller Ag-particles is much higher due to their higher specific surface area, thereby, higher silver ion release.[26,31,45] Furthermore, the bactericidal behaviour of Ag nanoparticles vanishes at larger diameters, *i.e.*, above 50–60 nm for *E. coli*.[26,31]

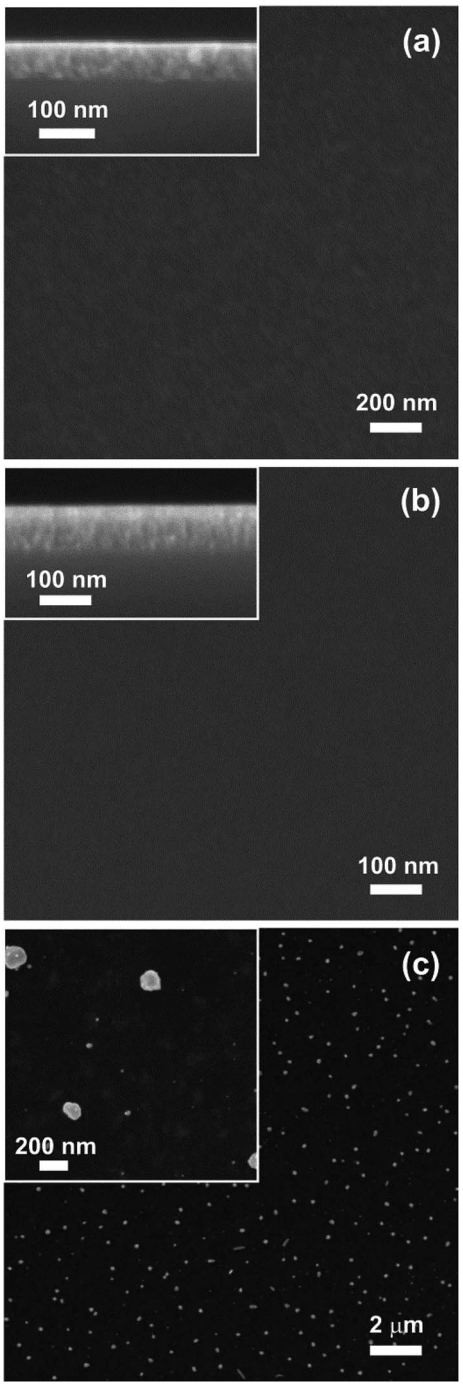

Fig. 3 FESEM images of various titania coatings: top-view of (a) TiO_2 type and (b) $pTiO_2$–*1 M* $AgNO_3$ type samples, the insets show the cross-sectional images. (c) Overview of the TiO_2–$AgNO_3$ type sample's surface. The inset shows an area in higher magnification.

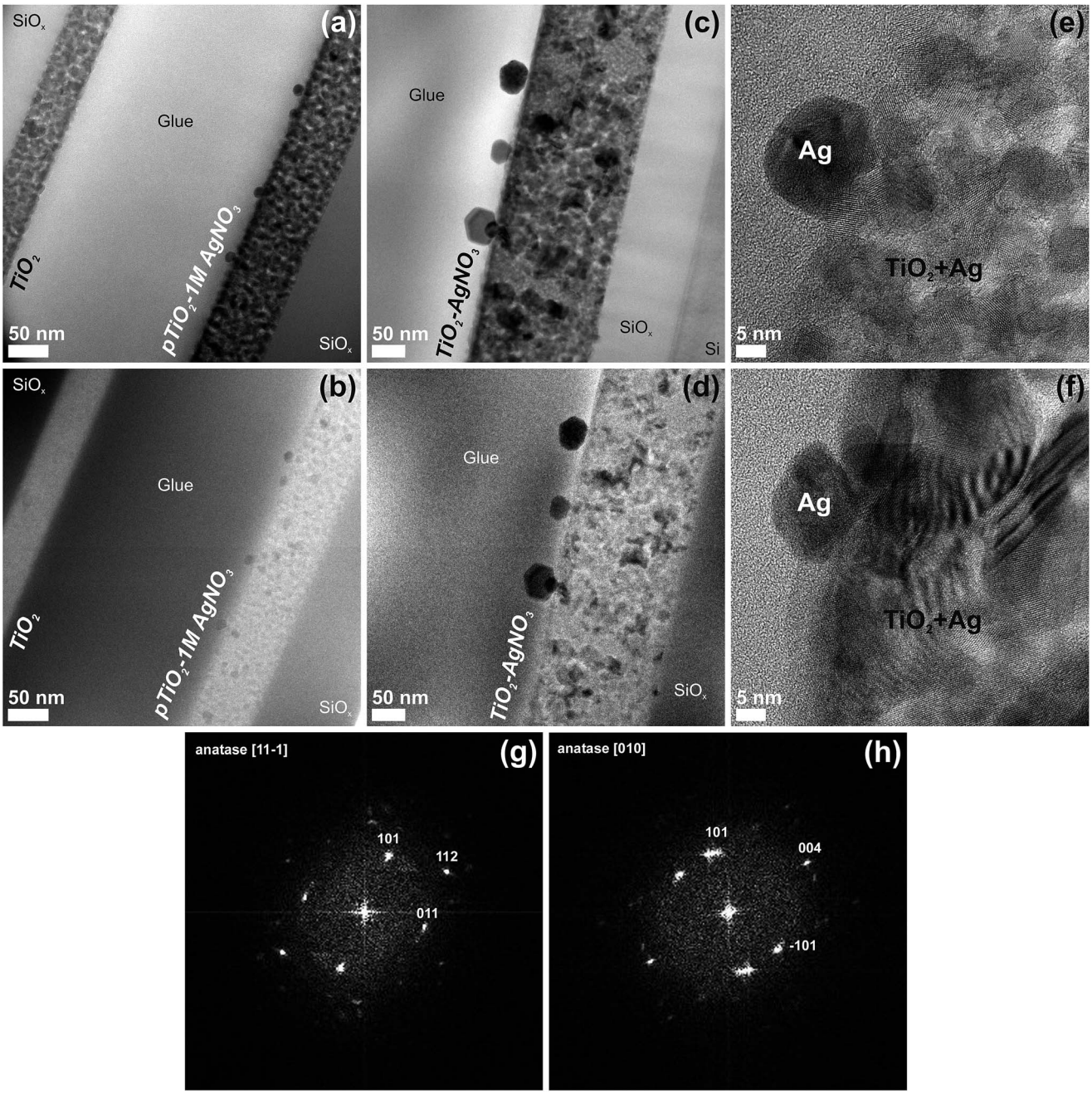

Fig. 4 Cross-sectional (a) TEM and (b) EELS images of TiO_2 (left) and $pTiO_2$–1 M $AgNO_3$ (right) type samples. Cross-sectional (c) TEM and (d) EELS images of TiO_2–$AgNO_3$ type sample. HRTEM images of (e) $pTiO_2$–1 M $AgNO_3$ and (f) TiO_2–$AgNO_3$ type samples. Images in (g) and (h) show the representative fast Fourier transforms from the images in (e) and (f), respectively, that reveals the anatase phase.

The visible light induced photocatalytic activity of the titania coatings as an effect of silver additive cannot be identified in the case of antibacterial tests. Statistical analysis was carried out by two-sample *t*-test and *p*-values were determined to strengthen this statement. The results of CFU assay obtained for irradiated coatings were compared with the cell viability values of samples kept in the dark. *p*-values exceeding 0.05 were considered not statistically significant. Statistically significant difference was obtained only for the TiO_2 type sample ($p < 0.001$). For $pTiO_2$ type and all silver containing samples (TiO_2–$AgNO_3$, $pTiO_2$–0.03 M $AgNO_3$, $pTiO_2$–1 M $AgNO_3$, $pTiO_2$–2*1 M $AgNO_3$) *p*-value was found to be higher than 0.05.

Consequently, there is no significant difference in the results of antibacterial tests carried out in the dark and under visible illumination. This result can be attributed to the fact that the effect of silver content overwhelms the photocatalytic contribution to the antibacterial behaviour of composite coatings in the visible wavelength range.

Results of the agar diffusion test. Agar diffusion tests were carried out for titania samples with and without silver additive

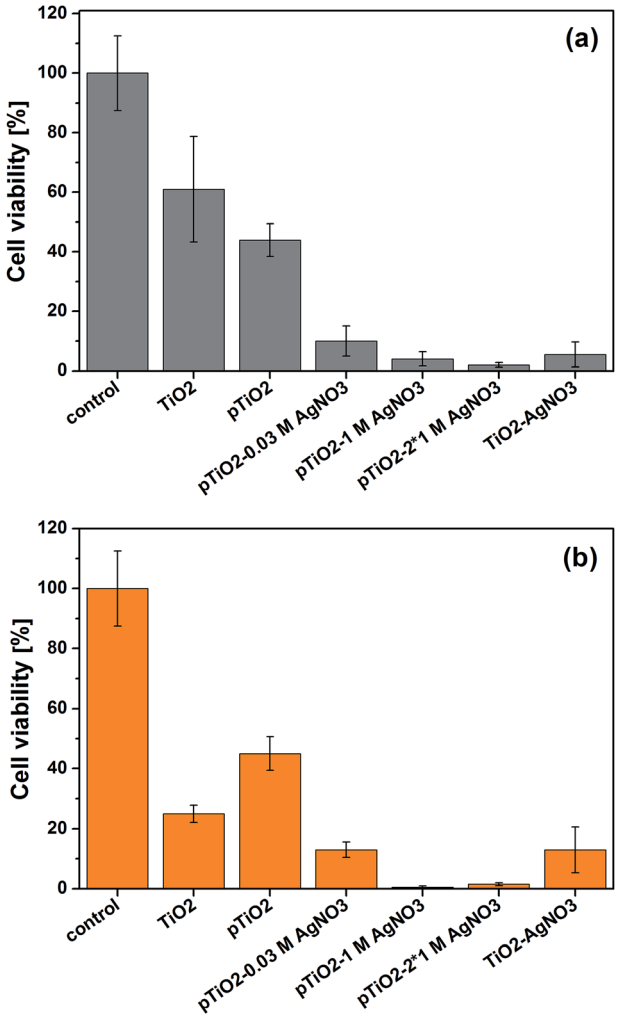

Fig. 5 Cell viability determined by CFU assay on different types of samples (a) kept in the dark and (b) irradiated with visible light. Cell viability [%] was calculated using $(N/N_0) \times 100$, where N_0 and N are the average number of 9 parallel CFUs obtained for the control glass substrate and for the investigated sample, respectively.

in the dark. The investigated samples were placed onto the surface of the agar plates containing *E. coli* bacteria cells, and then incubated at 37 °C for 24 hours. In the case of agar diffusion method an inhibition zone appears around the sample if the antibacterial material is able to diffuse from the sample into the nutrient agar. The size of the zone of inhibition is affected by the concentration and rate of diffusion of antibacterial agents from the coating into the agar.

Fig. 6 demonstrates the result of the agar diffusion test for $pTiO_2$ and $pTiO_2$–*0.03 M* $AgNO_3$ type samples, while Table 3 summarizes the results of the agar diffusion test of all types of samples.

Inhibition zones with about the same width appear only in the case of silver containing samples prepared *via* impregnation. There is no observable inhibition zone either in the case of titania coatings without silver additive or around the TiO_2–$AgNO_3$ type sample.

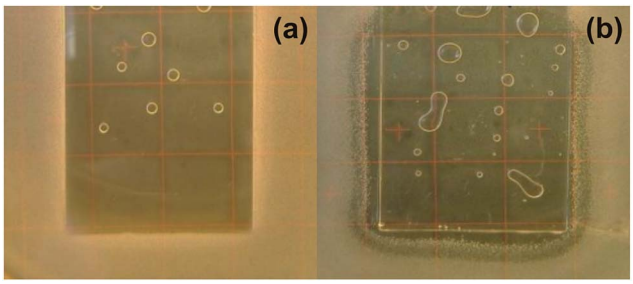

Fig. 6 Photographs taken of the (a) $pTiO_2$ type and (b) $pTiO_2$–*0.03 M* $AgNO_3$ type samples after performing the agar diffusion test.

These results show close agreement with those obtained for the CFU assay and refer to the fact that the diffusion of the silver content is easier from the pore structure ($pTiO_2$–$AgNO_3$ type coatings) than from the bulk material (TiO_2–$AgNO_3$ type sample). The results also demonstrate that the release of silver ions is not effective from the larger Ag particles carried by the surface of TiO_2–$AgNO_3$ type sample.

Durability and silver content of TiO_2 coatings

Silver content. The silver content of the coatings was determined by Rutherford backscattering spectrometry. Fig. 7 presents the initial silver content and its value after different soaking periods of 2 hours, 4 hours, 10 hours, and 20 hours – imitating consecutive antibacterial tests. The silver content of as-prepared samples corresponds to the expectations based on the way of sample preparation and results of the CFU assay experiments. The silver content of the as-prepared coatings can be estimated theoretically as well. In the case of $pTiO_2$–$AgNO_3$ type samples the calculation was done supposing that the total opened pore volume (24.6% porosity, determined by EP) is filled up by the aqueous $AgNO_3$ bulk solution. For TiO_2–$AgNO_3$ type sample the silver content was calculated based on the composition, *i.e.*, the Ag content of the precursor sol. Table 4 presents the initial silver content calculated theoretically and measured by RBS.

The experimentally determined silver content of samples is in a satisfactory agreement to our expectations. The lowest and highest silver amounts are detected for $pTiO_2$–*0.03 M* $AgNO_3$ and for TiO_2–$AgNO_3$ samples, respectively. The silver content of $pTiO_2$–*0.03 M* $AgNO_3$ is surprisingly high *cf.* the calculated value. Similarly, the measured values are consistently higher for the

Table 3 Width of the inhibition zone around different types of samples according to the agar diffusion antibacterial test

Sample	Width of the inhibition zone [mm]
TiO_2	0
$pTiO_2$	0
$pTiO_2$–0.03 M $AgNO_3$	2.3 ± 0.3
$pTiO_2$–1 M $AgNO_3$	2.3 ± 0.2
$pTiO_2$–2*1 M $AgNO_3$	2.2 ± 0.1
TiO_2–$AgNO_3$	0

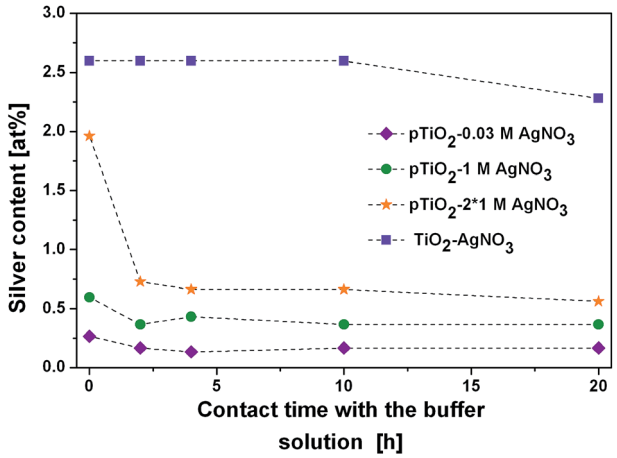

Fig. 7 Silver content of the coatings as a function of contact time with phosphate buffer solution measured by Rutherford backscattering spectrometry.

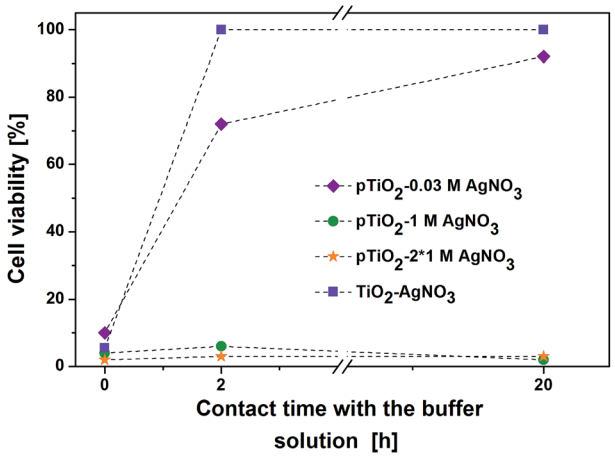

Fig. 8 Cell viability on the surface of different samples as a function of contact time.

impregnated samples. It refers to the possible accumulation of silver ions in the molecular-templated porous TiO_2 during the impregnation.

CFU assay. In order to study the durability of the silver containing titania coatings, samples were soaked with 200 μL phosphate buffer solution for 2 hours and 20 hours that was followed by the study of their antibacterial activity in the dark by CFU assay (Fig. 8).

All silver containing samples show similar and significant antibacterial activity at the first use. In case of *$pTiO_2$–0.03 M $AgNO_3$* type coating the activity decreases significantly after soaking the samples for 2 hours and shows further decrease after 20 hours. Contrarily, the antibacterial behaviour remains near constant for other impregnated samples (*$pTiO_2$–1 M $AgNO_3$*, *$pTiO_2$–2*1 M $AgNO_3$*) even after 20 hours contact time. The antibacterial activity of *TiO_2–$AgNO_3$* sample vanishes after 2 hours soaking. Consequently, the best antibacterial behaviour from the viewpoint of repeated application is shown by the samples prepared by impregnating the porous titania coatings with 1 M $AgNO_3$ solution once or twice (*$pTiO_2$–1 M $AgNO_3$* and *$pTiO_2$–2*1 M $AgNO_3$*).

Agar diffusion. The soaking experiment was followed up by the agar diffusion test for the two samples which showed long lasting antibacterial property (see Fig. 9).

The width of the inhibition zones decreases after the first use for both samples then it remains more or less constant – similarly to the results of CFU assay. This finding shows that these porous samples release enough silver ions even after 20 hours soaking time to reach or exceed the minimum inhibitory concentration of Ag (323 μg L^{-1} against *E. coli*[46]).

It is interesting to assess the minimum decrease of silver content of these samples in the agar diffusion tests supposing a box profile of silver ion distribution. We should consider the experimentally obtained widths of inhibition zones (Table 3) for reaching the minimum inhibitory concentration of Ag even at the border of the zone. In that case the minimum decrease of silver content in the layers is 0.09 at%. For CFU assay the decrease is even lower, 0.0075 at%, considering the volume of applied buffer solution (200 μL).

Discussion of correspondences. As can be seen, the silver content of the *$pTiO_2$–$AgNO_3$* type samples decreases significantly in the first 2 soaking hours and thereafter it stabilizes at a constant value (Fig. 7). Comparing the results presented in

Table 4 Silver content of the as prepared samples estimated theoretically and determined by RBS

Sample	Theoretically estimated silver content [at%]	Silver content determined by RBS [at%]
$pTiO_2$–0.03 M $AgNO_3$	0.007	0.265
$pTiO_2$–1 M $AgNO_3$	0.229	0.596
$pTiO_2$–2*1 M $AgNO_3$	0.455	1.961
TiO_2–$AgNO_3$	3.282	2.597

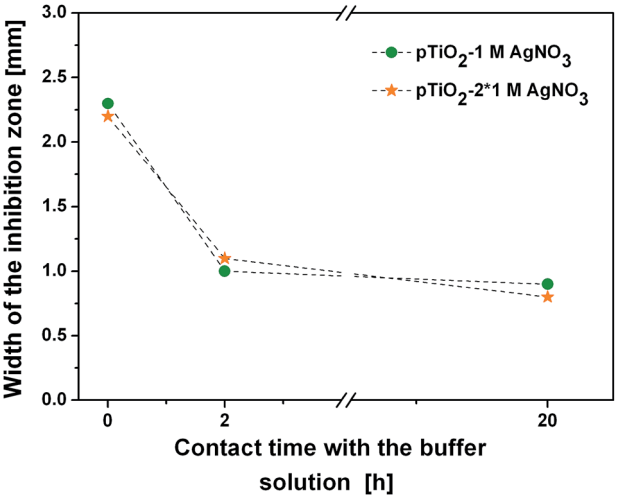

Fig. 9 Width of the inhibition zone around *$pTiO_2$–1 M $AgNO_3$* type and *$pTiO_2$–2*1 M $AgNO_3$* type samples according to the agar diffusion antibacterial test after different soaking periods.

Fig. 7 and 8 a correspondence between the antibacterial activity and silver content of $pTiO_2$–$AgNO_3$ samples can be established. In case of these samples the silver content decreases much more than the above estimated values during the first application. It means that the amount of released silver ions highly exceeds the minimum inhibitory concentration in the first antibacterial tests. The coating with the lowest silver content ($pTiO_2$–*0.03 M* $AgNO_3$), however, loses its antibacterial activity after the first use and the remaining silver content (0.16 at%) seems to be non-active in the antibacterial examinations. Although the mechanism is not completely clear it can be anticipated that some part of silver is in a bound form in the pores. The antibacterial activity of the $pTiO_2$–*1 M* $AgNO_3$ and $pTiO_2$–*2*1 M* $AgNO_3$ type samples remains suitable at the investigated time scale with a roughly constant silver content (0.36 at% and 0.56 at%, respectively).

Contrarily, the Ag content of TiO_2–$AgNO_3$ type samples does not change significantly even after 20 hours contact time, although their antibacterial activity ceases after the first use. It means that the antibacterial activity of this sample can only be attributed to Ag particles formed (in small amount) on the surface of coatings during the preparation. After the first application these particles presumably are removed from the surface hence antibacterial activity in the repeated applications cannot be observed. It seems that the Ag content in the layer is not available for the bacteria. The immigration of Ag-ions from the layer is hindered according to the fact that this sample cannot show any antibacterial activity in the agar diffusion tests (Table 3). Therefore, the silver particles on this coating can only kill bacteria in terms of contact mechanism.

Conclusions

The role of silver-doping methods was investigated in the long-term antibacterial activity of Ag–TiO_2 composite coatings. The effect of the nature and amount of the silver dopant, structural properties of the composite coatings was studied on the durability of antibacterial behaviour.

The TiO_2 coatings *per se* show antibacterial effect and the Ag content improves significantly this behaviour. For the molecular-templated porous ($pTiO_2$–$AgNO_3$ type) coatings the antibacterial effect correlates with the amount of the Ag content impregnated into the mesopore system. There is no significant increase in the photocatalytic activity of the samples upon visible light illumination. This can be attributed to the fact that the effect of Ag content overwhelms the photocatalytic contribution to the antibacterial behaviour of composite coatings. The Ag content of the impregnated coatings decreases fast during the first antibacterial tests due to the release of Ag ions and consequently their amount highly exceeds the minimum inhibitory concentration at the first use. The value of Ag content settles at a near constant value which is proportional to its initial quantity. The impregnated samples with the lowest silver content ($pTiO_2$–*0.03 M* $AgNO_3$) however lose their antibacterial activity after the first use; the remaining Ag content (0.16 at%) is not active in further examinations. Samples with higher Ag content remain active against bacteria in repeated tests even after 20 hours. These advantageous properties can be attributed to the nature of the Ag content due to the impregnation of the pore structure and the size-limiting character of the mesopores: the Ag content is distributed in the pore system and proved to be available in the antibacterial test.

Samples containing Ag in the bulk TiO_2 matrix (TiO_2–$AgNO_3$) do not show increased antibacterial activity despite their higher Ag content. The Ag content of these samples does not change even after 20 hours contact time but their antibacterial activity vanishes after the first use. The explanation was found in the character of the Ag content. The surface of these samples carries several crystalline particles: the typical dimension is above *ca.* 100 nm and a few small particles (<50 nm). According to literature, the bactericidal activity of Ag nanoparticles against *E. coli* can be attributed to the smaller size fraction (below 50–60 nm). The antibacterial activity of this sample can only be attributed to these particles formed in small amount on the surface of coatings. After the first application these particles are presumably removed from the surface hence antibacterial activity cannot be observed in the repeated applications. Although Ag occurs in the coating material with a dimension smaller than the above mentioned threshold value, it is not available for the bacteria. According to the agar diffusion tests the release of Ag-ions from the layer is apparently blocked and these samples can only kill bacteria by direct contact. Hence, impregnated molecular-templated coatings are good candidates for coating implants and in applications against drop infection.

Acknowledgements

The authors thank A. Bánkuti, A. Deák, E. Hild, R. Jancsek, V. Kovács-Kiss, K. Pázsi, D. Zámbó, and Z. Zwickl for their help in this work. The financial support of the National Development Agency (Hungarian-French Bilateral Co-operation, PHONOSEL, TéT_11-2-2012-0008) and Hungarian Scientific Research Fund (OTKA K 112114) is gratefully acknowledged. The research work has been accomplished in the framework of the "BME R + D + I project", supported by the grant TÁMOP 4.2.1/B-09/1/KMR-2010-0002. Emőke Albert's research work was supported by the European Union and the State of Hungary, co-financed by the European Social Fund in the framework of TÁMOP-4.2.4.A/2-11/1-2012-0001 "National Excellence Program".

References

1 T. Matsunaga, R. Tomoda, T. Nakajima and H. Wake, *FEMS Microbiol. Lett.*, 1985, **29**, 211.
2 J. G. McEvoy and Z. Zhang, *J. Photochem. Photobiol., C*, 2014, **19**, 62.
3 R. van Grieken, J. Marugán, C. Sordo, P. Martínez and C. Pablos, *Appl. Catal., B*, 2009, **93**, 112.
4 O. Akhavan, *J. Colloid Interface Sci.*, 2009, **336**, 117.
5 O. Akhavan and E. Ghaderi, *Surf. Coat. Technol.*, 2010, **204**, 3676.
6 K. Page, R. G. Palgrave, I. P. Parkin, M. Wilson, S. L. P. Savin and A. V. Chadwick, *J. Mater. Chem.*, 2007, **17**, 95.

7 Y. Liu, X. Wang, F. Yang and X. Yang, *Microporous Mesoporous Mater.*, 2008, **114**, 431.
8 G. Fu, P. S. Vary and C. T. Lin, *J. Phys. Chem. B*, 2005, **109**, 8889.
9 J. C. Yu, W. Ho, J. Yu, H. Yip, P. K. Wong and J. Zhao, *Environ. Sci. Technol.*, 2005, **39**, 1175.
10 B. Ohtani, *Chem. Lett.*, 2008, **37**, 217.
11 M. R. Hoffman, S. T. Martin, W. Choi and D. W. Bahnemann, *Chem. Rev.*, 1995, **95**, 69.
12 J. Ma, Z. Xiong, T. D. Waite, W. J. Ng and X. S. Zhao, *Microporous Mesoporous Mater.*, 2011, **144**, 97.
13 I. A. Shkrob and M. C. Sauer Jr, *J. Phys. Chem. B*, 2004, **108**, 12497.
14 M. Anpo, S. Kishiguchi, Y. Ichihashi, M. Takeuchi, H. Yamashita, K. Ikeue, B. Morin, A. Davidson and M. Che, *Res. Chem. Intermed.*, 2001, **27**, 459.
15 C. Burda, Y. Lou, X. Chen, A. C. S. Samia, J. Stout and J. L. Gole, *Nano Lett.*, 2003, **3**, 1049.
16 G. Zhao, H. Kozuka and T. Yoko, *Thin Solid Films*, 1996, **277**, 147.
17 J. M. Herrmann, H. Tahiri, Y. Ait-Ichou, G. Lassaletta, A. R. González-Elipe and A. Fernández, *Appl. Catal., B*, 1997, **13**, 219.
18 M. Li, M. E. Noriega-Trevino, N. Nino-Martinez, C. Marambio-Jones, J. Wang, R. Damoiseaux, F. Ruiz and E. M. V. Hoek, *Environ. Sci. Technol.*, 2011, **45**, 8989.
19 M. P. Reddy, A. Venugopal and M. Subrahmanyam, *Water Res.*, 2007, **41**, 379.
20 X. Bingshe, N. Mei, W. Liqiao, H. Wensheng and L. Xuguang, *J. Photochem. Photobiol., A*, 2007, **188**, 98.
21 J. Husheng, H. Wensheng, W. Liqiao, X. Bingshe and L. Xuguang, *Dent. Mater.*, 2008, **24**, 244.
22 W. R. Li, X. B. Xie, Q. S. Shi, H. Y. Zeng, Y. S. Ou-Yang and Y. B. Chen, *Appl. Microbiol. Biotechnol.*, 2010, **85**, 1115.
23 C.-N. Lok, C.-M. Ho, R. Chen, Q.-Y. He, W.-Y. Yu, H. Sun, P. K.-H. Tam, J.-F. Chiu and C.-M. Che, *J. Proteome Res.*, 2006, **5**, 916.
24 S. L. Percival, P. G. Bowler and D. Russell, *J. Hosp. Infect.*, 2005, **60**, 1.
25 T. Yuranova, A. G. Rincon, A. Bozzi and S. Parra, *J. Photochem. Photobiol., A*, 2003, **161**, 27.
26 S. Eckhardt, P. S. Brunetto, J. Gagnon, M. Priebe, B. Giese and K. M. Fromm, *Chem. Rev.*, 2013, **113**, 4708.
27 C. Marambio-Jones and E. M. V. Hoek, *J. Nanopart. Res.*, 2010, **12**, 1531.
28 H. T. Ratte, *Environ. Toxicol. Chem.*, 1999, **18**, 89.
29 V. Sambhy, M. M. MacBride and B. R. Peterson, *J. Am. Chem. Soc.*, 2006, **128**, 9798.
30 R. M. Slawson, M. I. van Dyke, H. Lee and J. T. Trevors, *Plasmid*, 1992, **27**, 72.
31 A. Panacek, L. Kvitek, R. Prucek, M. Kolar, R. Vecerova, N. Pizurova, V. K. Sharma, T. Navecna and R. Zboril, *J. Phys. Chem. B*, 2006, **110**, 16248.
32 K. N. Thakkar, S. S. Mhatre and R. Y. Parikh, *J. Nanomed. Nanotechnol.*, 2010, **6**, 257.
33 J. S. Grewal and R. P. Tiwari, *J. Med. Microbiol.*, 1990, **32**, 223.
34 E. Volentiru, M. Nyári, G. Szabó, Z. Hórvölgyi and L. M. Mureşan, *Period. Polytech., Chem. Eng.*, 2014, **58**, 61.
35 E. Albert, N. Cotolan, N. Nagy, G. Sáfrán, G. Szabó, L. M. Mureşan and Z. Hórvölgyi, *Microporous Mesoporous Mater.*, 2015, **206**, 102.
36 A. Venkateswara Rao, A. B. Gurav, S. S. Latthe, R. S. Vhatkar, H. Imai, C. Kappenstein, P. B. Waghd and S. C. Gupta, *J. Colloid Interface Sci.*, 2010, **352**, 30.
37 A. Mills and S. L. Hunte, *J. Photochem. Photobiol., A*, 1997, **108**, 1.
38 M. Bellantone, H. D. Williams and L. L. Hench, *Antimicrob. Agents Chemother.*, 2002, **16**, 1940.
39 Y. L. Wang, Y. Z. Wan, X. H. Dong, G. X. Chen, H. M. Tao and T. Y. Wen, *Carbon*, 1998, **36**, 1567.
40 C. Trapalis, N. Todorova, M. Anastasescu, C. Anastasescu, M. Stoica, M. Gartner, M. Zaharescu and T. Stoica, *Thin Solid Films*, 2009, **517**, 6243.
41 S. A. Tomás, A. Luna-Resendis, L. C. Cortés-Cuautli and D. Jacinto, *Thin Solid Films*, 2009, **518**, 1337.
42 E. Kótai, *Nucl. Instrum. Methods Phys. Res., Sect. B*, 1994, **85**, 588.
43 B. Ohtani, O. O. Prieto-Mahaney, D. Li and R. Abe, *J. Photochem. Photobiol., A*, 2010, **216**, 179.
44 S. J. Gregg and K. S. W. Sing, *Adsorption, Surface area and Porosity*, Academic Press, New York, 2nd edn, 1982.
45 C. Baker, A. Pradhan, L. Pakstis, D. J. Pochan and S. I. J. Shah, *J. Nanosci. Nanotechnol.*, 2005, **5**, 244.
46 C.-N. Lok, C.-M. Ho, R. Chen, Q.-Y. He, W.-Y. Yu, H. Sun, P. K.-H. Tam, J.-F. Chiu and C.-M. Che, *J. Biol. Inorg. Chem.*, 2007, **12**, 527.